


## Article

# *Scutellaria baicalensis* Flavones as Potent Drugs against Acute Respiratory Injury during SARS-CoV-2 Infection: Structural Biology Approaches

Ana-Maria Udrea <sup>1,2</sup> , Maria Mernea <sup>1,\*</sup>, Cătălin Buiu <sup>3,\*</sup> and Speranța Avram <sup>1</sup>

<sup>1</sup> Department of Anatomy, Animal Physiology and Biophysics, Faculty of Biology, University of Bucharest, 91–95 Splaiul Independenței, 050095 Bucharest, Romania; m.a.u.anamaria@gmail.com (A.-M.U.); speranta.avram@gmail.com (S.A.)

<sup>2</sup> Laser Department, National Institute for Laser, Plasma and Radiation Physics, Atomistilor Street, No. 409, P.O. Box MG-36, RO-077125 Magurele City, Romania

<sup>3</sup> Department of Automatic Control and Systems Engineering, Politehnica University of Bucharest, 313 Splaiul Independenței, 060042 Bucharest, Romania

\* Correspondence: maria.mernea@bio.unibuc.ro (M.M.); catalin.buiu@upb.ro (C.B.)

Received: 13 October 2020; Accepted: 13 November 2020; Published: 16 November 2020



**Abstract:** Severe acute respiratory syndrome coronavirus 2 (SARS-CoV-2) infection can result in severe damage to the respiratory system. With no specific treatment to date, it is crucial to identify potent inhibitors of SARS-CoV-2 Chymotrypsin-like protease (3CLpro) that could also modulate the enzymes involved in the respiratory damage that accompanies SARS-CoV-2 infection. Here, flavones isolated from *Scutellaria baicalensis* (baicalein, baicalin, wogonin, norwogonin, and oroxylin A) were studied as possible compounds in the treatment of SARS-CoV-2 and SARS-CoV-2-induced acute lung injuries. We used structural bioinformatics and cheminformatics to (i) identify the critical molecular features of flavones for their binding activity at human and SARS-CoV-2 enzymes; (ii) predict their drug-likeness and lead-likeness features; (iii) calculate their pharmacokinetic profile, with an emphasis on toxicology; (iv) predict their pharmacodynamic profiles, with the identification of their human body targets involved in the respiratory system injuries; and (v) dock the ligands to SARS-CoV-2 3CLpro. All flavones presented appropriate drug-like and kinetics features, except for baicalin. Flavones could bind to SARS-CoV-2 3CLpro at a similar site, but interact slightly differently with the protease. Flavones' pharmacodynamic profiles predict that (i) wogonin strongly binds at the cyclooxygenase2 and nitric oxide synthase; (ii) baicalein and norwogonin could modulate lysine-specific demethylase 4D-like and arachidonate 15-lipoxygenase; and (iii) baicalein, wogonin, norwogonin, and oroxylin A bind to SARS-CoV-2 3CLpro. Our results propose these flavones as possible potent drugs against respiratory damage that occurs during SARS-CoV-2 infections, with a strong recommendation for baicalein.

**Keywords:** infections; antiviral; flavonoids; pharmacokinetics; pharmacodynamic; SARS-CoV-2; *Scutellaria baicalensis*; bioinformatics

## 1. Introduction

One of the severe acute respiratory syndrome coronavirus 2 (SARS-CoV-2) pandemic challenges is the optimal treatment and prevention of severe injuries in the human lung. An evaluation of patients showed that SARS-CoV-2 infection induces viral pneumonia that leads to acute lung injuries in up to 20% of symptomatic patients [1,2]. Acute lung injuries, resulting from the acute onset of symptoms, including severe hypoxia and noncardiogenic pulmonary edema, have been shown to display a death rate of over 50% [3].

Additionally, SARS-CoV-2 infection may lead to a more severe form of lung disorder, called acute respiratory distress syndrome [3]. It has been shown that Coronavirus disease 2019 (COVID-19) is associated with a “sepsis-like inflammation or a cytokine storm” determined by immune system hyperactivation [4] and with acute respiratory distress syndrome [5]. Recent histopathological studies have demonstrated the critical role of endothelial cells in vascular dysfunction, immunothrombosis, and inflammation in severe SARS-CoV-2 infections [6].

Recently, endothelitis with diffuse endothelial inflammation, as well as micro- and macrovascular thrombosis, both in the venous and arterial circulations, particularly pulmonary embolism, was observed in COVID-19 patients [6]. On the other hand, severe COVID-19 infection has been associated with strong cytokine secretion and immune cell recruitment that resulted in endothelial cell activation [6].

Considering the critical role of endothelial cells in maintaining lung homeostasis and vascular permeability, it was supposed that any dysfunction at an endothelial cell level actively leads to thrombo-inflammatory processes that ultimately result in COVID-19 vasculopathy and ventilation-perfusion mismatch [7].

Several enzymes are activated during the acute respiratory distress induced by SARS-CoV-2 infection, with some of them being (i) lysine-specific demethylase 1 (LSD1) [8], which serves as a pro-fibrotic regulator in pulmonary fibrosis; (ii) xanthine dehydrogenase (XDH) [9], critical in the degradation of purine and hypoxia during inflammation [10]; (iii) arachidonate 15-lipoxygenase (ALOX15) [11], with importance in the inflammatory response, probably through regulating the macrophage function and actin polymerization; (iv) cyclin-dependent kinase 1 (CDK1) [12], a protein that is very important in the eukaryote cell cycle; (v) cyclooxygenase (COX) [13], important in both the physiological and pathological state of the lung [14]; and (vi) inducible nitric oxide synthase (iNOS) [15].

Other proteins involved in lung disorders are cytokines and chemokines, with important roles in immunity and immunopathology during influenza or coronavirus infections [16]. Patients diagnosed with severe COVID-19 exhibited increased levels of pro-inflammatory cytokines, especially the soluble interleukin 2 receptor (IL-2R), interleukin-6 (IL-6), and tumor necrosis factor- $\alpha$  (TNF- $\alpha$ ) [17].

The study of Rossaint et al. [18] showed that ALOX15 is directly involved in the recruitment of neutrophils in diverse lung compartments during pulmonary inflammation and strong ALOX15 inhibitors could be a new approach in the treatment of acute lung injury. CDK1 and CDK2 inhibitors may represent a new therapy in lung cancer, leading to anaphase catastrophe in lung cancer cells and preventing inflammation [19]. Moreover, it was mentioned that COX inhibitors can reduce the early changes in lung mechanics, but do not prevent capillary injury.

Studies on animal models support the idea that iNOS inhibitors can be used in the treatment of cancer, autoimmune, or inflammatory disorders [20]. iNOS is also overexpressed in the lungs after lipopolysaccharide treatment.

In addition to the human enzymes discussed above, efficient anti-SARS-CoV-2 drugs should also target SARS-CoV-2 enzymes [17,21–23]. The Chymotrypsin-like protease (viral 3CLpro) is responsible for the maturation of non-structural proteins, which is a process that is essential for the virus life cycle. Therefore, it represents a very attractive target in SARS-CoV-2 treatment.

Bioinformatics tools were used to predict the effect of natural compounds on human enzymes, such as LSD1, XDH, ALOX15, CDK1, COX, and iNOS, as well as on the viral 3CLpro. By employing this approach, we intended to identify compounds with both antiviral activity and beneficial effects on the lung damage that accompanies SARS-CoV-2 infection.

Based on our expertise in the bioinformatics of antiviral drugs [24] and also in the bioinformatics of natural compounds [25], we aimed to search for natural compounds with dual functions, employing ligands for both human and viral enzymes presented above.

We focused our study on *Scutellaria baicalensis* compounds [26,27], with an emphasis on the flavonoids norwogonin, oroxylin A, baicalein, baicalin, and wogonin (Figure 1). *S. baicalensis* is a traditional medicinal plant that has been used in the last 2000 years in China for the treatment of many

pathologies, such as cancer, colds, pneumonia, respiratory infections, microbial infections, and brain disorders [28]. Approximately 63 different flavonoids were isolated from *S. baicalensis*, with some of them being baicalein, wogonin, tenaxin, norwogonin, oroxylin A, skullcapflavone, etc. [29].

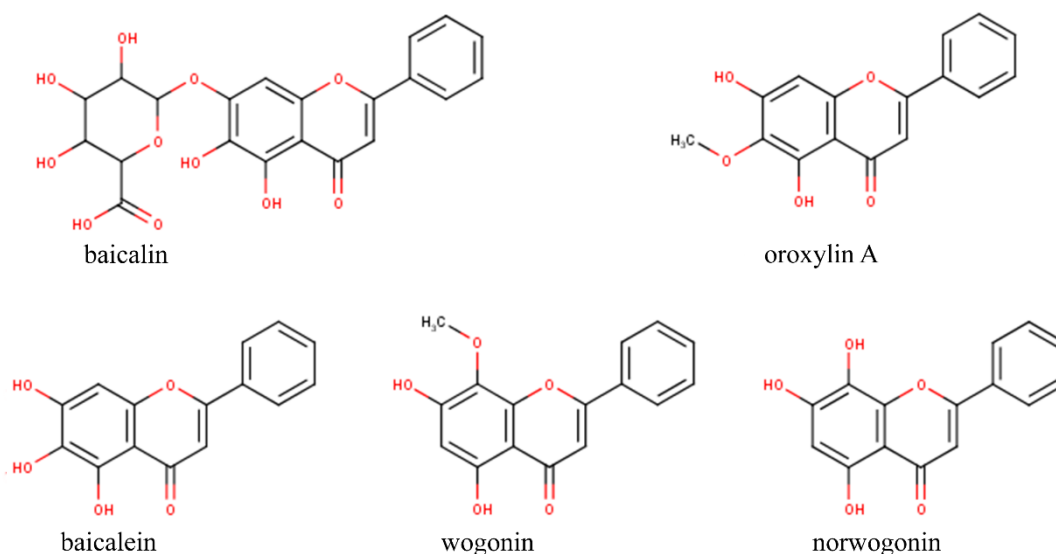


**Figure 1.** Chemical structure of the flavonoids baicalin, oroxylinA, baicalein, wogonin, and norwogonin from *Scutellaria baicalensis*.

Diagrams of norwogonin, oroxylinA, baicalein, baicalin, and wogonin structures, as well as some of their chemical features, are presented in Table 1 [30] and Figure 1.

**Table 1.** The International Union of Pure and Applied Chemistry (IUPAC) name, hydrophobicity (XLogP3), molecular weight, hydrogen bond donor count, and hydrogen bond acceptor count of baicalein, baicalin, wogonin, norwogonin, and oroxylin A [30].

Compounds	IUPAC Name	XLogP3	Molecular Weight g/mol	H-Bond Donor	H-Bond Acceptor
baicalein	5,6,7-trihydroxy-2-phenylchromen-4-one	1.7	270.24	3	5
baicalin	(2S,3S,4S,5R,6S)-6-(5,6-dihydroxy-4-oxo-2-phenylchromen-7-yl)oxy-3,4,5-trihydroxyoxane-2-carboxylic acid	1.1	446.4	6	11
wogonin	5,7-dihydroxy-8-methoxy-2-phenylchromen-4-one	3	284.26	2	5
norwogonin	5,7,8-trihydroxy-2-phenylchromen-4-one	2.7	270.24	3	5
oroxylin A	5,7-dihydroxy-6-methoxy-2-phenylchromen-4-one	2.1	284.26	2	5

In Table 1, we present the chemical features of these compounds, namely, the hydrophobicity (XLogP3), molecular weight, hydrogen bond donor count, and hydrogen bond acceptor count. We noticed that (i) the chemical compounds are described by hydrophobic features, as their XLogP3 values range from 3 (wogonin) to 1.1 (baicalin); (ii) norwogonin, oroxylinA, baicalein, and wogonin presented very similar accounts of the hydrogen bond donor and hydrogen bond acceptor (Table 1), unlike baicalin (hydrogen bond donor count = 6 and hydrogen bond acceptor = 11); and (iii) the molecular weights are very similar for norwogonin, oroxylinA, baicalein, and wogonin (molecular weight varies from 270.24 to 284.26 g/mol), but not for baicalin (MW = 446.4 g/mol).

The remarkably close values of the chemical features of norwogonin, oroxylinA, baicalein, and wogonin may be explained by the common presence of 2-phenylchromen-4-one in their chemical structures and very discrete variation of substituents (see Table 1, IUPAC name).

Baicalein is known for its antimicrobial and anti-inflammatory effects [31], having a beneficial effect on the symptoms of acute respiratory distress [32]. Baicalein could have a possible inhibitory mechanism for lipoxygenase, CDK, and COX-2 [32].

Wogonin [33] can also be used in the treatment of acute respiratory distress, acting on nuclear factor kappa B (NF- $\kappa$ B) and COX-2 [34]. Norwogonin presents antiviral activity on enterovirus 71 [35], while oroxylin A displays therapeutic activity in pathologies such as bacterial/viral infections [35], without a precise known molecular mechanism. The synergic effects of baicalein, wogonin, and oroxylin A at NF- $\kappa$ B were previously studied [34].

Here, we identified the biological activity of baicalein, baicalin, wogonin, norwogonin, and oroxylin A in the respiratory system and obtained their complete pharmacologic profiles (kinetics and dynamics). Important structural features such as the electronic features represented by orbital energies, dipole moment, interaction field area, and charge-weighted positive/negative surface area were obtained to determine the ligand profiles of these compounds and to predict their beneficial effect in lung injuries.

A large part of the study was dedicated to describing the human proteins and SARS-CoV-2 3CLpro as targets for baicalein, wogonin, norwogonin, and oroxylin A by applying computed targets probability and molecular docking. Special attention was given to human proteins strongly expressed in the lung, such as LSD1, XDH, ALOX15, CDK1, COX, and iNOS. At the end of this paper, we propose an action mechanism of these compounds in preventing lung injury during viral infection.

## 2. Materials and Methods

### 2.1. Ligand Preparation

We selected five flavonoids from *S. baicalensis*, baicalein, baicalin, wogonin, norwogonin, and oroxylin A. These compounds may have SARS-CoV-2 3CLpro inhibitor activity; at the same time, these could be beneficial against lung damage associated with a viral infection.

Several studies have pointed out the anti-SARS-CoV-2 effects of *S. baicalensis* compounds, with an emphasis on baicalein and baicalin [36–40], wogonin [39], and oroxylin A [39].

Song et al. [37] revealed that baicalein significantly inhibited replication of the virus and relieved the lesions of lung tissue in hACE2 transgenic mice infected with SARS-CoV-2. Moreover, Huang [41] noticed that baicalein and wogonin could be employed as the main active ingredients for the management of COVID-19 by targeting ACE2 and 3CLpro proteins. The compounds also inhibited inflammatory mediators, regulating immunity and eliminating free radicals through COX-2, CASP3, or IL-6.

Taking these studies into account, we selected baicalein, baicalin, wogonin, and oroxylin A for further analysis. Because of the structural similarity to wogonin and a known antiviral activity against a enterovirus 71 [35], norwogonin was also included in the group of flavonoids that we decided to analyze in this study.

The Simplified Molecular Input Line Entry (SMILES) files of selected compounds were retrieved from the PubChem database [30] and used for further bioinformatic and cheminformatic analysis (Table 2).

The spatial structures of compounds were refined in Molecular Operating Environment 13 (MOE 13) software [42] by performing energy minimization using the MMFF94x force field and a 0.005 gradient. Afterward, all the chemical compounds were converted to a mol2 chemical format using MOE software. The nonpolar hydrogen molecules were merged with the carbons, with polar hydrogen charges of the Gasteiger-type being assigned.

**Table 2.** Chemical name, PubChem ID, SMILES files, and chemical–disease associations.

Chemical Name	PubChem ID	SMILES	Chemical-Disease Associations
baicalein	5281605	<chem>C1=CC=C(C=C1)C2=CC(=O)C3=C(O2)C=C(C(=C3O)O)O</chem>	liver injury, fibrosis, glioblastoma, hyperalgesia
baicalin	64982	<chem>C1=CC=C(C=C1)C2=CC(=O)C3=C(C(=C(C(=C3O2)OC4C(C(C(C(O4)C(=O)O)O)O)O)O)O)O</chem>	kidney injury, brain ischemia, fibrosis, inflammation, liver cirrhosis
wogonin	5281703	<chem>COC1=C(C=C(C2=C1OC(=CC2=O)C3=CC=CC=C3)O)O</chem>	kidney injury, acute lung injury edema, gastrointestinal, neoplasms, glioma
norwogonin	5281674	<chem>C1=CC=C(C=C1)C2=CC(=O)C3=C(O2)C=C(C(=C3O)O)O</chem>	HIV-1 antiviral
oroxylin A	5320315	<chem>COC1=C(C2=C(C(=C1O)OC(=CC2=O)C3=CC=CC=C3)O</chem>	bacterial infections, bradycardia, hypotension, inflammation

## 2.2. Assessment of Compounds' Drug- and Lead-Likeness Features

To evaluate the drug- and lead-likeness features, baicalein, baicalin, wogonin, norwogonin, and oroxylin A were subjected to Lipinski [43], Ghose [44], Veber [45], and Egan [46] filters using the SwissADME webservice [47].

When applying these filters, bioactive drugs are expected not to violate more than one of the criteria for drug-likeness and lead-likeness: (i) The molecular weight should be no greater than 500, the coefficient of partition between octanol and water (Log P(o/w)) should be no more than 5, the number of hydrogen bond acceptors should be no more than 10, and the number of hydrogen bond donors should be no more than 5 (Lipinski's filter); (ii) the molecular weight should be between 160 and 480, the Log P(o/w) should be between −0.4 and 5.6, the molar refractivity should be between 40 and 130, and the number of atoms should be between 20 and 70 (Ghose filter); (iii) the number of rotatable bonds should be no more than 10 and the total polar surface area should be no greater than 140 (Veber filter); (iv) the Log P(o/w) should be no more than 5.88 and the total polar surface area should be no greater than 131.6 (Egan filter). The compounds that respected all of the criteria were retained in the study and were subjected to the following investigations.

## 2.3. Compounds' Predicted Molecular Features and Pharmacophore Fingerprint Search

The molecular features of flavones were calculated using the descriptor computation facility of MOE 13 [42]. Due to the discrete structural differences between baicalein, wogonin, norwogonin, and oroxylin A, we identified the most critical molecular features of the compounds that could best describe their therapeutic effects in lung inflammation and fibrosis.

We selected the critical molecular features considering no redundancy and the non-correlation of independent variables. Based on our previous studies [24,48] and literature data, from the 200 molecular features that we initially calculated, only a few of them were taken into account for further analysis, including the electronic features represented by orbital energies (AM1\_HOMO, AM1\_LUMO), dipole moment (AM1\_dipole), interaction field area (vsurf\_S), and charge-weighted positive/negative surface area (CASA+, CASA−).

Additionally, the functional similarity of baicalein, wogonin, norwogonin, and oroxylin A was addressed by ruling MOE/Similarity Search using the Graph 3-Point Pharmacophore fingerprint field [49] and Tanimoto coefficients [50].

## 2.4. Compounds' Computational Pharmacodynamic Profiles

The pharmacodynamic features and possible molecular mechanisms by which baicalein, baicalin, wogonin, norwogonin, and oroxylin A modulate SARS-CoV-2 protease and human enzymes involved in lung damage are missing from bioinformatic and pharmaceutical databases.



In this context, Swiss TargetPrediction [51] was used to establish the probability of baicalein, baicalin, wogonin, norwogonin, and oroxylin A presenting binding affinities for enzymes that play a specific role in inflammatory infections and damages of the lung.

The interaction of flavones with 3CLpro was investigated based on the crystal structure of 3CLpro bound to baicalein—PDB:6M2N [40,52].

The docking of flavones to a subunit of 3CLpro, namely chain A, was performed with SwissDock [53], which is a web service based on the EADock DSS engine [54], by applying the Accurate docking type. The Dock Prep module in Chimera [55] was used for preparing the docking target and the ligand structures downloaded from the Chemical Entities of Biological Interest (ChEBI) database [56].

From the resulting docking solutions, we selected the poses that best overlapped the location of baicalein in the 6M2N structure for further analysis. Protein–ligand interaction maps for baicalein based on the 6M2N structure and for wogonin, norwogonin, and oroxylin A, based on the docking results, were calculated using LigPlot+ [57].

### 2.5. Computational ADME-Tox Profiles of Natural Compounds

Predicted Absorption Distribution Metabolism Excretion (ADME) profiles of baicalein, baicalin, wogonin, norwogonin, and oroxylin A were developed using the pkCSM database [58] and ProTox [59] prediction service based on their chemical SMILES files.

From the ADME items, we selected the following: (i) Intestinal absorption (human, %)—a molecule with an absorption of less than 30% is considered to be poorly absorbed; (ii) Caco-2 Permeability (LogPapp, cm/s)—molecules are considered to have a high Caco-2 permeability if  $P_{app} > 8 \times 10^{-6}$  cm/s; (iii) blood–brain barrier (BBB) permeability expressed as the logarithm of the brain to plasma drug concentration ratio—log BBB of more than 0.3 indicates good BBB permeability, whilst a value of less than −1 indicates low BBB permeability; (iv) central nervous system (CNS) permeability, where a compound with a permeability-surface area product (logPS) higher than −2 is penetrating the CNS; and (v) the CYP3A4 substrate (3A4 is one of the isoforms of cytochrome P450 responsible for the metabolism of a drug) and total clearance (renal and hepatic clearance) [58].

Using pkCSM and ProTox web servers, we evaluated the Salmonella typhimurium reverse mutation assay AMES toxicity, hepatotoxicity, hERG (potassium channels encoded by hERG genes) affinity, LD50 (median lethal dose), immunotoxicity, cytotoxicity, nuclear receptor signaling pathways as active/inactive on the aryl hydrogen receptor (AhR), and stress response pathways as active/inactive on the mitochondrial membrane potential (MMP) and phosphoprotein tumor suppressor (p53) [58,59].

## 3. Results and Discussion

### 3.1. Drug-Likeness, Lead-Likeness, and ADME-Tox Features

The results generated from the medicinal chemistry filtering (Lipinski, Ghose, Veber, and Egan) and ADME-Tox analyses are represented in Table 3, Figure 2, and Table 4. Our results revealed that baicalein, wogonin, norwogonin, and oroxylin A comply with drug-likeness rules, suggesting that these flavones have possible drug actions and good bioavailability.

**Table 3.** The bioavailability, drug-likeness, and lead-likeness features of baicalein, baicalin, wogonin, norwogonin, and oroxylin A.

Compounds	Lipinski	Ghose	Veber	Egan	Lead-Likeness
baicalein	yes	yes	yes	yes	yes
baicalin	no	yes	no	no	no
wogonin	yes	yes	yes	yes	yes
norwogonin	yes	yes	yes	yes	yes
oroxylin A	yes	yes	yes	yes	yes

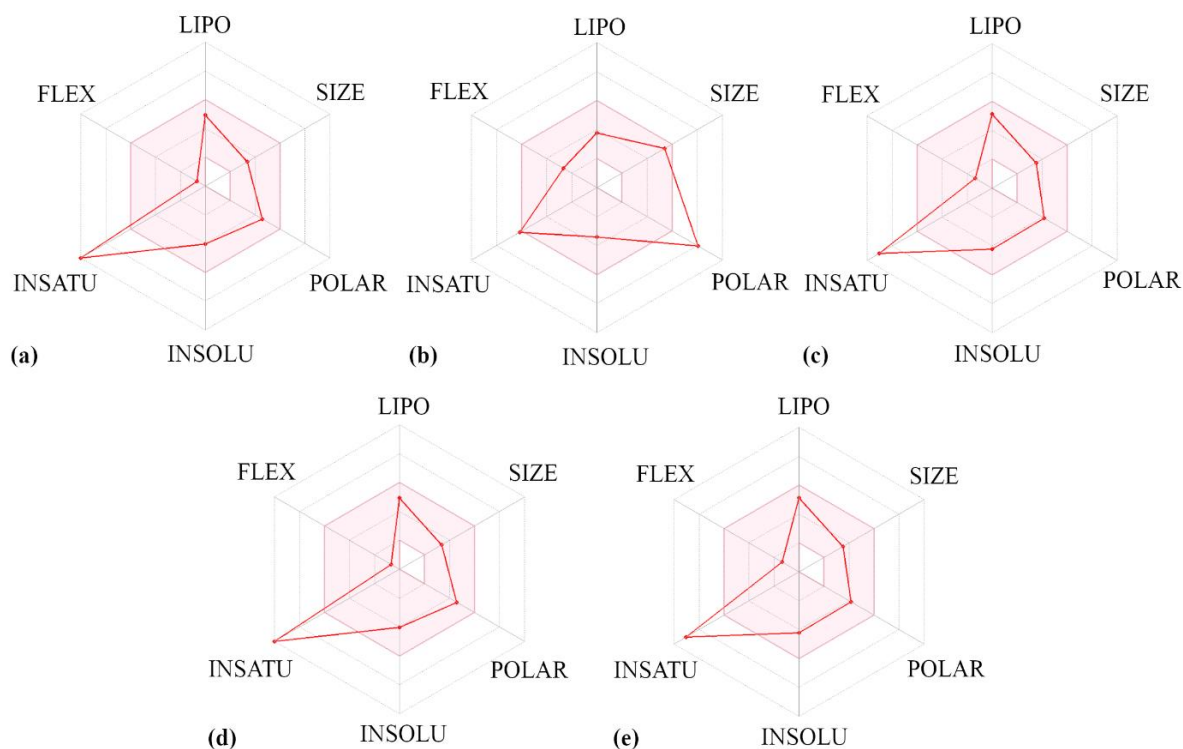


**Figure 2.** The bioavailability radar of baicalein (a), baicalin (b), wogonin (c), norwogonin (d), and oroxylin A (e) predicted using SwissADME [51].

Instead, baicalin presented two violations of Lipinski's rule (number of H-Bond acceptors (respectively 11, see Table 1) greater than 10 and number of H-Bond donors greater than 5 (respectively 6, see Table 1)) and one violation of Veber's rule (a total polar surface area greater than 140). Furthermore, baicalin exhibited a violation of lead-likeness rules, namely, a molecular weight of more than 350.

The bioavailability radar of baicalein, baicalin, wogonin, norwogonin, and oroxylin A obtained in SwissADME [51] showed a fast evaluation of drug-likeness. The bioavailability radar included six physicochemical properties: (i) The lipophilicity (XLOGP3 between  $-0.7$  and  $+5.0$ ); (ii) size (molecular weight between 150 and 500 g/mol); (iii) polarity (a total polar surface area between 20 and 130 Å<sup>2</sup>); (iv) solubility (not higher than 6); (v) saturation (fraction Csp3 not lower than 0.25); and (vi) flexibility (the number of rotatable bonds is not more than 9) [51].

The pink area represents the optimal range of these properties [60] and the red line represents the properties of natural compounds. In Figure 2, it can be observed that the red lines of baicalein, wogonin, norwogonin, and oroxylin A are in the range of the pink area. Therefore, we can conclude that these compounds are predicted as orally bioavailable.

**Table 4.** Predicted ADME-Tox features of baicalein, baicalin, wogonin, norwogonin, and oroxylin A. Their probability of exhibiting toxicity features is mentioned in brackets.

ADME	Baicalein	Baicalin	Wogonin	Norwogonin	Oroxylin A
<b>ABSORPTION</b>					
Caco2 permeability numeric (log Papp in 10 <sup>−6</sup> cm)	1.11	−0.67	0.96	1.10	1.02
Intestinal absorption (human) numeric (% absorbed)	94.26	26.22	92.68	94.48	94.34
P-glycoprotein substrate	yes	yes	yes	yes	yes
<b>DISTRIBUTION</b>					
Fraction unbound (human) (Fu)	0.15	0.29	0.10	0.14	0.082
BBB permeability (log BBB)	−1.06	−1.33	−2.23	−0.96	−0.11
CNS permeability (Log PS)	−2.21	−3.81	−2.18	−2.15	−2.21
<b>METABOLISM</b>					
CYP1A2 inhibitor	yes	no	yes	yes	yes
CYP2D6 substrate/inhibitors	no	no	no	no	no
CYP3A4 substrate/inhibitors	no	no	yes	no	yes
<b>EXCRETION</b>					
Total clearance (log mL/min/kg)	0.25	0.04	0.29	0.25	0.31
Renal OCT2 substrate	no	no	no	no	no
<b>TOXICITY</b>					
hepatotoxicity	inactive (0.69)	inactive (0.75)	inactive (0.72)	inactive (0.69)	inactive (0.72)
carcinogenicity	active (0.68)	active (0.50)	active (0.68)	active (0.68)	inactive (0.68)
immunotoxicity	inactive (0.99)	inactive (0.92)	inactive (0.80)	inactive (0.96)	inactive (0.81)
mutagenicity	active (0.51)	inactive (0.68)	inactive (0.94)	active (0.51)	inactive (0.94)
cytotoxicity	inactive (0.99)	inactive (0.91)	inactive (0.95)	inactive (0.99)	inactive (0.95)
hERG I/II inhibitors	no	no	no	no	no
activity on aryl hydrogen receptor	active (0.91)	inactive (0.60)	inactive (0.60)	active (0.91)	active (0.97)
activity on mitochondrial membrane potential	active (1.00)	inactive (0.63)	active (0.92)	active (1.00)	active (0.92)
activity on phosphoprotein tumor suppressor (p53)	inactive (0.97)	inactive (0.89)	inactive (0.86)	inactive (0.97)	inactive (0.86)
Max. tolerated dose (human) (log mg/kg/day)	0.49	0.65	0.15	0.48	−0.08

Furthermore, the ADME-predicted features of natural compounds were computed (Table 4). We evaluated the ADME features, with an emphasis on (i) intestinal absorption and Caco-2 permeability; (ii) BBB permeability, considering that these compounds target the enzymes expressed in the lung; and (iii) the type of cytochrome for which these compounds are substrates/inhibitors and a renal organic cation transporter 2 (OCT2) substrate.

The results of the predicted ADME profiles showed that baicalein, wogonin, norwogonin, and oroxylin A have very good intestinal absorption (ranging from 92.68 to 94.48), unlike baicalin, which exhibited unexpectedly low intestinal absorption. Concerning Caco2 permeability, all five flavones presented a good permeability.



The considered natural compounds recorded middle BBB permeability values (log BBB varied from  $-2.23$  to  $-0.11$ ). In the central nervous system, baicalein, wogonin, norwogonin, and oroxylin A have an appropriate CNS permeability, varying from  $-2.15$  to  $-2.21$ .

Of the analyzed compounds, oroxylin A presented a suitable permeability at BBB and also a good permeability in the nervous system, while wogonin presented a weaker possibility to cross the BBB barrier. Our results agree with experimental data [61] showing that baicalin attenuates blood–brain barrier disruption and hemorrhagic transformation and improves neurological outcomes in ischemic stroke rats. Generally, compounds from *S. baicalensis* have beneficial effects on BBB permeability during hypoxia [62].

Regarding the probability of studied flavones to bind plasma proteins, we recorded exceedingly small values of unbound fractions for all five compounds. Our results regarding the metabolism pathways showed that the studied flavones are CYP1A2 inhibitors, except for baicalin, and that none of the five flavones are CYP2D6 substrates or inhibitors. Our results are sustained by an experimental study [63] which mentioned that wogonin was a potent, competitive inhibitor of CYP1A2 ( $K_i = 0.24 \mu\text{M}$ ), and a weak inhibitor of CYP2C19 ( $\text{IC}(50) = 101.10 \mu\text{M}$ ), but was not able to inhibit CYP2C9, CYP2D6, CYP2E1, and CYP3A4 ( $\text{IC}(50) > 200 \mu\text{M}$ ). Important results were recorded for the elimination rate, demonstrating that none of the five flavones are renal OCT2 substrates.

In our study, high importance was given to the prediction of the compounds' toxicity. Our results revealed that (i) none of the compounds present hepatotoxicity, immunotoxicity, cytotoxicity, and cardiotoxicity, and (ii) carcinogenicity may be induced by baicalein, baicalin, wogonin, and norwogonin, but not oroxylin A. Our results agree with very recent studies mentioning low hepatotoxicity [29,31,64]. AMES was negative for all compounds studied here.

It was also important to analyze the activity of compounds at the aryl hydrogen receptor and also on the phosphoprotein tumor suppressor (p53). Our results showed that baicalein, norwogonin, and oroxylin A are very active at the aryl hydrogen receptor, while all compounds are inactive on p53. Moreover, our results allow us to state that baicalein, wogonin, norwogonin, and oroxylin A are very active on the mitochondrial membrane potential.

### 3.2. Predicted Molecular Features of Flavones and Their Pharmacophore Fingerprint Search

By extending our previous studies regarding the molecular descriptors of natural compounds in various disorders [25], we analyzed the molecular descriptors that are considered important for the antimicrobial and anti-inflammatory activities of the studied flavones (Table 5). By computing the molecular orbital energies of baicalein, baicalin, wogonin, norwogonin, and oroxylin A, we noticed that no significant variation was recorded for lowest unoccupied molecular orbital (LUMO) energies, which varied from  $-0.77 \text{ eV}$  (baicalin) to  $-0.67 \text{ eV}$  (norwogonin).

**Table 5.** Molecular features of natural compounds isolated from *Scutellaria baicalensis*.

Compounds	AM1-LUMO eV	AM1-HOMO eV	vsurf_S $\text{\AA}^2$	CASA_POS $\text{\AA}^2$	CASA_NEG $\text{\AA}^2$
baicalein	$-0.71$	$-8.93$	417.42	577.84	337.03
baicalin	$-0.77$	$-8.83$	592.19	1655.53	945.98
wogonin	$-0.70$	$-9.03$	445.75	671.13	287.35
norwogonin	$-0.67$	$-8.78$	418.22	579.01	327.94
oroxylin A	$-0.73$	$-9.12$	443.53	689.63	282.60

Remarkably close values were recorded for LUMO energies of baicalein, wogonin, and oroxylin A. The analyses of Highest Occupied Molecular Orbital (HOMO) energies recorded variation between  $-9.12 \text{ eV}$  (oroxylinA) and  $-8.78 \text{ eV}$  (norwogonin). An interesting observation was noted, in that the HOMO energy of baicalein ( $-8.93 \text{ eV}$ ) was extremely close to the HOMO energy of norwogonin

(−8.78 eV), while the HOMO energy of wogonin (−9.03 eV) and oroxylin A (−9.12 eV) presented remarkably similar values (Table 5).

Other important molecular descriptors that we considered here were the surface exposed at receptors and solvent ( $vsurf\_S$ ), and the surface areas formed around positive and negative atoms. Our results showed that  $vsurf\_S$  significantly varies from 592.19 Å<sup>2</sup> to 417.42 Å<sup>2</sup>, and the fields of the interaction areas of baicalein ( $vsurf\_S = 417.42$  Å<sup>2</sup>) and norwogonin ( $vsurf\_S = 418.22$  Å<sup>2</sup>) are similar, while wogonin and oroxylin A have very close values for the field of the interaction area (Table 5). Analyzing the distribution of positive/negative charges is important during the interaction of flavones with human enzymes and viral enzymes.

Our results showed that the molecular descriptor CASA\_POS significantly varies from 1655.53 Å<sup>2</sup> (baicalin) to 577.84 Å<sup>2</sup> (baicalein). Close values of CASA\_POS were recorded for norwogonin (579.01 Å<sup>2</sup>) and baicalein, while wogonin and oroxylin A had similar values for CASA\_POS (Table 5). Additionally, we calculated CASA\_NEG. Similar values were recorded for the pairs baicalein (337.03 Å<sup>2</sup>) and norwogonin (327.94 Å<sup>2</sup>) and wogonin (287.35 Å<sup>2</sup>) and oroxylin A (282.60 Å<sup>2</sup>).

The strong similarity of the chemical structures of the studied compounds requires a complete analysis of the spatial distribution of critical features, such as the electrostatic or amphiphilic potential (hydrophobic and hydrophilic) on the surface area. This would lead to a better understanding of the interaction between these flavones with enzyme targets involved in lung injuries (Figure 2). The values of Table 5 are sustained in Figure 3.

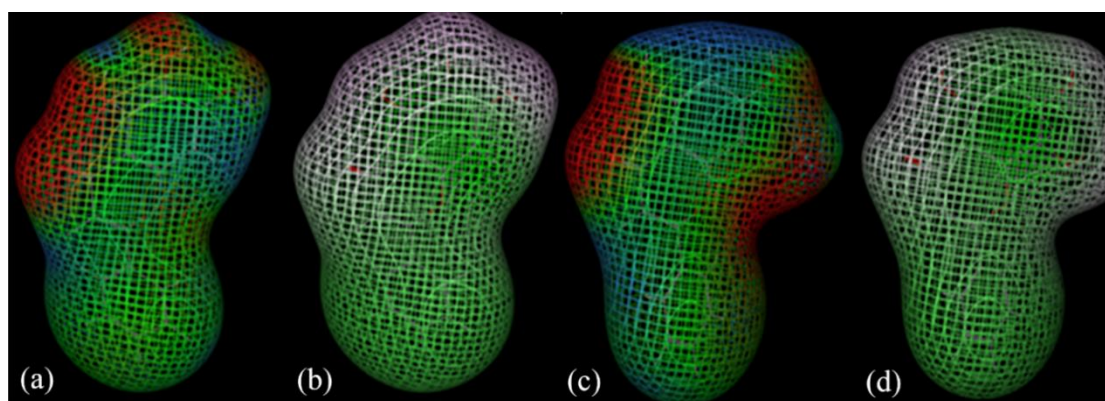


**Figure 3.** The spatial distribution of features of baicalein (a,b) and wogonin (c,d). In (a,c), electrostatic potentials are represented (red indicates negative and blue indicates positive) and in (b,d), amphiphilic potentials are represented (green indicates hydrophobic, violet indicates hydrophilic, and white indicates neutral).

We observed a large distribution of positive charges on wogonin in comparison with baicalein (blue zones) and a large hydrophobic area (green) around wogonin, with this distribution being in agreement with the Log P(o/w) calculated for wogonin (2.80) versus baicalein (2.40). Besides the calculation of the molecular descriptors, we also evaluated the functional similarity of baicalein, wogonin, norwogonin, and oroxylin A using Tanimoto similarity coefficients, with a gradual increase from 30 to 50 (Table 4), choosing fingerprint field-3D Pharmacophore Points, with wogonin as the template structure. We consider that performing a similarity analysis on synthetic and natural compounds may not only reveal the possible spatial similarity/non-similarity between these compounds, but also offers a new perspective on the interpretation of their biological activities. Our results showed that pharmacophore similarity was recorded for wogonin, baicalein, norwogonin, and oroxylin A at Tanimoto coefficient = 30%; wogonin, norwogonin, and oroxylin A at Tanimoto coefficient = 60%, and wogonin and norwogonin at Tanimoto coefficient = 70%.

### 3.3. Computational Pharmacodynamic Profiles of Baicalein, Wogonin, Norwogonin, and Oroxylin A

The structure of SARS-CoV-2 3CLpro bound to baicalein was solved by Su et al. [40]. The authors identified baicalein as a novel nonpeptidomimetic compound that inhibits SARS-CoV-2 3CLpro with micromolar potency, with the  $IC_{50}$  being 0.94  $\mu$ M. Baicalein presented a high affinity for the viral 3CLpro, with the  $K_d$  measured by isothermal titration calorimetry being 4.03  $\mu$ M and the calculated ligand efficiency being 0.37 kcal/mol [40]. The crystal structure determined by Su et al. [40] comprises four 3CLpro protomers that assemble as two dimers, with each protomer being bound by a baicalein molecule. Structurally, a 3CLpro protomer comprises domains I (residues 10 to 99), II (residues 100 to 182), and III (residues 198 to 303); Glu166 residues are important in shaping S1 pockets of substrate binding sites from the catalytically active 3CLpro dimer [65]. To describe the interaction of baicalein with a 3CLpro dimer (chains A and C), in Figure 4a, we present their protein–ligand interaction maps. It is interesting to note that the two baicalein molecules interact slightly differently in comparison to the two 3CLpro monomers.

Overall, baicalein molecules form multiple hydrophobic make contact with residues from domains I (residues His41 and Met49) and II (residues Asn142, Cys145, and Met165). The interaction also involves three hydrogen bonds with backbone nitrogen atoms of residues Gly143 and Glu166. Specifically, the baicalein molecule bound to chain A also forms hydrophobic contacts with residues Cys44 (domain I) and His164, Asp187, and Gln189 (domain II). The baicalein molecule bound to chain C forms a single additional hydrophobic contact with residue Leu141 (domain II). Wogonin, norwogonin, and oroxylin A are also expected to bind to 3CLpro. These flavones were docked at the baicalein binding site identified from the 6M2N crystal structure [40,52].

The SwissDock full fitness scores calculated for these compounds are −1257.99 for wogonin, −1267.92 for norwogonin, and −1261.69 for oroxylin A. These values are slightly lower than the full fitness score calculated for baicalein docked close to its binding site (−1271.18), suggesting that wogonin, norwogonin, and oroxylin A also bind favorably to 3CLpro, but less favorably than baicalein.

In the case of wogonin, norwogonin, and oroxylin A, protein–ligand interactions were analyzed on the complexes obtained by docking. The results are presented in Figure 4b–d. It is possible to observe that, in comparison to baicalein, the binding of wogonin, norwogonin, and oroxylin A to 3CLpro presents some particularities. Wogonin forms hydrophobic contacts with nearly the same residues as baicalein, but forms two hydrogen bonds with the sulfur atom from Cys145 and a hydrogen bond with a side chain oxygen from residue Glu166. Norwogonin binds to 3CLpro through hydrophobic interactions with residues shared with baicalein and with an additional residue, namely Thr25. Norwogonin forms a hydrogen bond with the backbone nitrogen atom of Gly143 and two hydrogen bonds with the sulfur atom of Cys145. Oroxylin A forms hydrophobic contacts with the same residues, but forms only two hydrogen bonds with the sulfur atom of Cys145. It appears that the considered flavones present similar binding sites, but the slight differences between their chemical structures induce differences in the interactions with residues from the site.

In their study, Su et al. [40] also addressed the binding of other compounds to SARS-CoV-2 3CLpro, with wogonin and oroxylin A being among them. The two compounds did not appear as 3CLpro inhibitors at the tested concentrations, but wogonin exhibited strong antiviral activity against SARS-CoV-2 in Vero E6 cells [40]. We believe additional experimental work is required to address the efficiency of the compounds in inhibiting 3CLpro, especially in the case of norwogonin, which was not tested in previous studies.

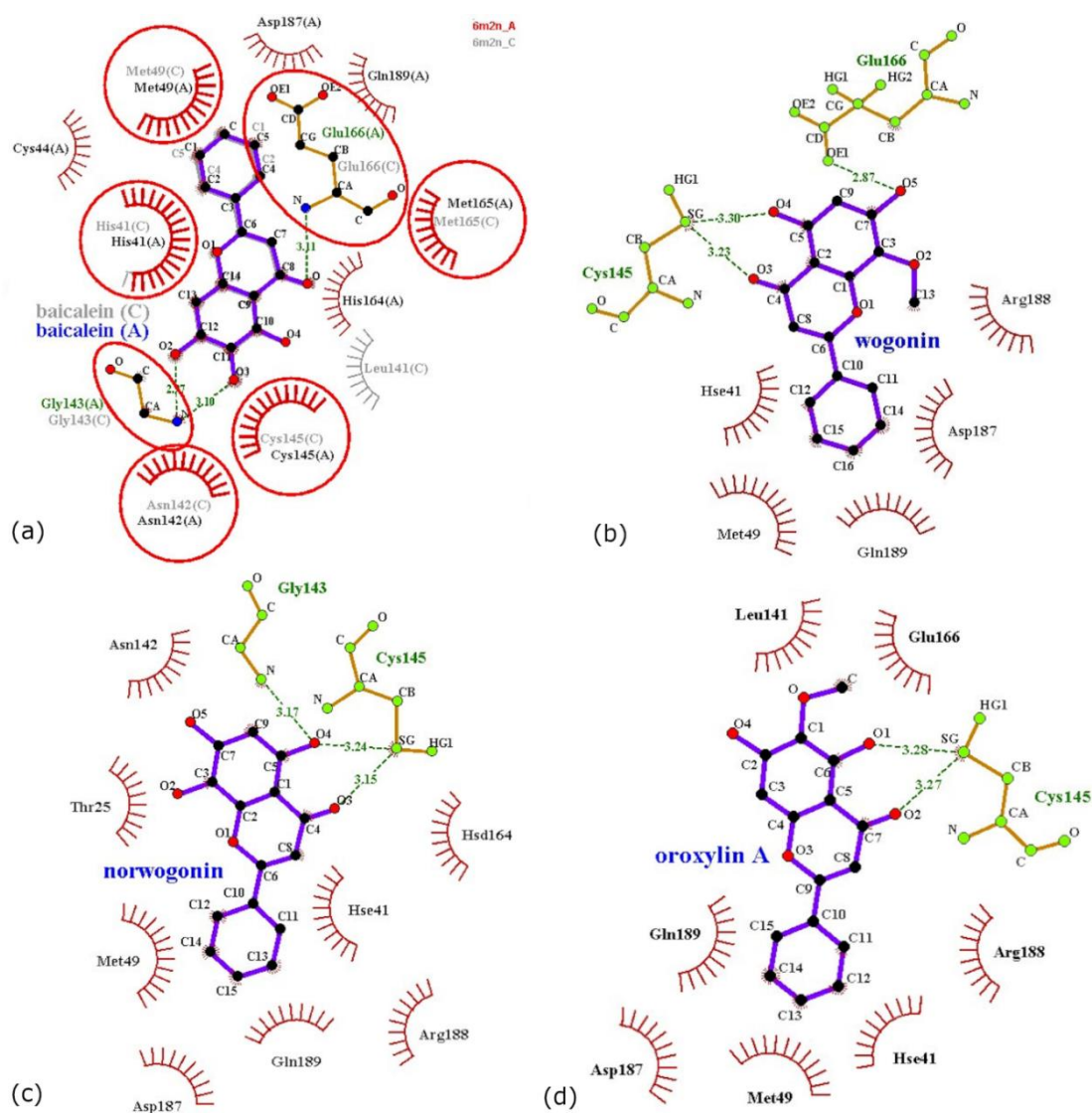


**Figure 4.** Protein–ligand interactions for Chymotrypsin-like protease (3CLpro) and baicalein (a), wogonin (b), norwogonin (c), and oroxylin A (d). Interactions mediated by hydrogen bonds (dashed lines) are presented in green and those mediated by hydrophobic contacts (arc with spokes) are presented in brown. The ligand is represented in purple and contacted atoms are shown with spokes. In (a), we superimposed the interaction maps of baicalein with two 3CLpro protomers that form a dimer in the crystal structure 6M2N, namely chain A (with red) and chain C (with gray). The chains are also labeled in brackets next to all residues from the figure.

Besides the viral target of flavones, it is particularly important to mention other possible human proteins involved in lung damage as flavones targets. In the introduction section, we mentioned six enzymes that are strongly involved in severe symptoms during lung disorders, namely lysine-specific demethylase 4D (KDM4D; we chose the KDM4D enzyme because of the lack of data regarding the LSD1 enzyme), XDH, ALOX15, CDK1, COX-2, and iNOS. The Swiss TargetPrediction server was used to predict the binding probability of the considered flavones for these enzymes.

The results presented in Table 6 show that baicalein displays a high affinity for enzymes strongly involved in lung injuries, such as KDM4D (maximum probability = 1), XDH (maximum probability = 1), ALOX15 (maximum probability = 1), and CDK1 (maximum probability = 1), but a very weak affinity for COX-2 (maximum probability = 0.25) and iNOS (maximum probability = 0.10). Our results are in agreement with experimental data [32].



**Table 6.** The human proteins included in respiratory disorders as targets for baicalein, baicalin, wogonin, norwogonin, and oroxylin A and their binding probability.

Enzymes	Baicalein Binding Probability	Wogonin Binding Probability	Norwogonin Binding Probability	Oroxylin A Binding Probability
KDM4D	1	-	0.60	0.18
XDH	1	0.10	0.60	0.18
ALOX15	1	0.13	0.62	0.19
CDK1	1	0.10	0.62	0.18
COX-2	0.30	1	0.17	0.30
iNOS	0.30	1	0.16	0.60

Similar results were obtained for norwogonin that interacts with a good probability with KDM4D-like, XDH, Arachidonate 15-lipoxygenase, and CDK1 (Table 6 and Figure 5). Interesting results for the binding probability were obtained for wogonin and oroxylin A, which show a good binding probability for COX-2 (wogonin maximum probability = 1, oroxylin A maximum probability = 0.30) and iNOS (wogonin maximum probability = 1, oroxylin A maximum probability = 0.60). Our results are in agreement with experimental data [34].

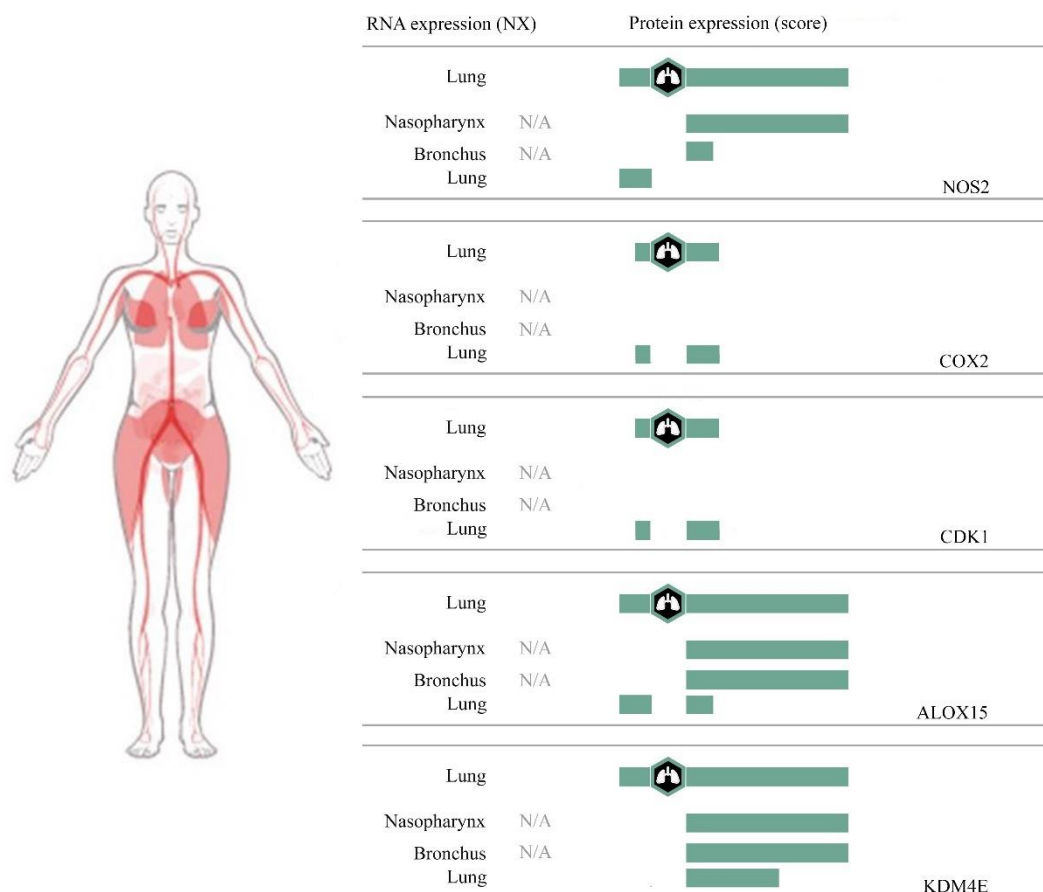


**Figure 5.** The expression of nitric oxide synthase 2 (NOS2), cyclooxygenase 2 (COX2), cyclin-dependent kinase 1 (CDK1), arachidonate 15-lipoxygenase (ALOX15), and lysine-specific demethylase 4E (KDM4E) in human respiratory segments.

Additionally, by accessing the Human Protein Atlas [66], we represented the expression of iNOS, CDK1, ALOX15, KDM4D-like enzyme KDM4E, and COX-2 in the nasopharynx, bronchia, and lung,

in order to elucidate whether the studied flavones can inhibit SARS-CoV-2 viral particles just at the open gate (nasopharynx and bronchia), before it arrives in the lung.

Figure 5 shows that ALOX15 and KDM4E, which is a lysine demethylase from the same family as KDM4D [67], are strongly expressed in the nasopharynx, bronchia, and lung, and we suppose that baicalein may be useful in reducing damage of the respiratory system that occurs just into the superior zone.

Furthermore, wogonin and oroxylin A that may interact with iNOS can reduce the damage induced by viral particles to the nasopharynx and bronchia.

By consulting the literature, we found some experimental results on the binding of compounds considered here to human protein targets, including XDH, ALOX15, CDK1, COX-2, iNOS, and LSD1. The data summarized in Table 7 mostly confirm our predictions discussed above. As can be seen, baicalein has been the most intensively investigated compound and is a known inhibitor of ALOX15, CDK1, COX-2, and LSD1. In our literature search, we could not find experimental data on norwogonin, showing that it has not been previously considered as a candidate inhibitor of these human proteins. The predictions performed here suggest that norwogonin should be taken into account in future studies.

**Table 7.** Experimental results obtained from the literature regarding the biological activity between human enzymes from our study and *S. baicalensis* flavones. The italics represent experimental data that differ from our prediction.

Enzymes	Baicalein Experimental Activity	Baicalin Experimental Activity	Norwogonin Experimental Activity	Wogonin Experimental Activity	Oroxylin A Experimental Activity
XDH	-	-	-	-	-
ALOX15	yes-inhibitor [68]	-	-	-	-
CDK1	yes-inhibitor [69]	yes-inhibitor [69,70]	-	-	<i>yes-inhibitor [71]</i>
COX-2	<i>yes-inhibitor [68]</i> not inhibited [72]	not inhibited [72]	-	yes-inhibitor [73] not inhibited [72] <i>not inhibited [73]</i> <i>not inhibited [72]</i>	-
iNOS	not inhibited [72]	not inhibited [72]	-	<i>not inhibited [73]</i> <i>not inhibited [72]</i>	-
LSD1	yes-inhibitor [74]	yes-inhibitor [75]	-	yes-inhibitor [74]	<i>yes-inhibitor [74]</i>

#### 4. Conclusions

In the present work, we focused on five promising flavone molecules isolated from *S. baicalensis*, namely baicalein, baicalin, wogonin, norwogonin, and oroxylin A. These flavones were considered as promising compounds for the fight against SARS-CoV-2 with a double function: As inhibitors of SARS-CoV-2 3CLpro and modulators of human enzymes that are responsible for lung damage that is seen in COVID-19 patients.

The flavones were extensively characterized by their drug- and lead-likeness features, their pharmacokinetic and pharmacodynamic profiles, and their molecular descriptors more relevant for their biological activities. All flavones except for baicalin presented appropriate drug-like and kinetic features. The analysis of molecular features and the pharmacophore fingerprint search showed a similarity between baicalein and norwogonin and between wogonin and oroxylin A.

Molecular docking demonstrated that baicalein, wogonin, norwogonin, and oroxylin A bind to the viral 3CLpro at similar sites, with particularities depending on their chemical structures. Literature data support the efficiency of baicalein in inhibiting SARS-CoV-2 3CLpro, while wogonin appears to be a strong antiviral that does not inhibit the protease. These compounds may represent possible ligands for enzymes involved in respiratory disorders. For instance, wogonin is strongly predicted to bind to COX-2 and iNOS.

The results presented here point to the idea that the investigated flavones could be used as potential antivirals and agents against lung damage that occurs during SARS-CoV-2 infections. Moreover, we suggest that baicalein is the best candidate characterized here.



**Author Contributions:** Conceptualization, M.M., A.-M.U., S.A., and C.B.; methodology, M.M. and A.-M.U.; software, A.-M.U., M.M., and S.A.; validation, S.A., M.M., and A.-M.U.; formal analysis, C.B.; investigation, A.-M.U. and M.M.; resources, A.-M.U.; data curation, S.A.; writing—original draft preparation, A.-M.U. and M.M.; writing—review and editing, C.B. and S.A.; visualization, A.-M.U.; supervision, S.A.; project administration, S.A.; funding acquisition, S.A. All authors have read and agreed to the published version of the manuscript.

**Funding:** This work was funded by the Romanian National Authority for Scientific Research and Innovation, CNCS/CCCDI-UEFISCDI [grant no PN-III-P1-1.1-PCCDI- 2017-0728].

**Conflicts of Interest:** The authors declare no conflict of interest.

## Abbreviations

Coronavirus disease 2019: COVID19; severe acute respiratory syndrome coronavirus 2: SARS-CoV-2; Chymotrypsin-like protease: 3CLproS; lysine-specific demethylase 1: LSD1; xanthine dehydrogenase: XDH; arachidonate 15-lipoxygenase: ALOX15; cyclin-dependent kinase 1: CDK1; cyclooxygenase: COX; inducible nitric oxide synthase: iNOS; soluble interleukin 2 receptor: IL-2R; interleukin-6: IL-6; tumor necrosis factor- $\alpha$ : TNF- $\alpha$ ; nuclear factor kappa B: NF- $\kappa$ B; coefficient of partition between octanol and water: Log P(o/w); International Union of Pure and Applied Chemistry: IUPAC; simplified molecular-input line-entry system: SMILES Molecular Operating Environment 13: MOE 13; electronic features represented by orbital energies: AM1\_HOMO/AM1\_LUMO; lowest unoccupied molecular orbital LUMO; Highest Occupied Molecular Orbital: HOMO; dipole moment: AM1\_dipole; interaction field area: vsurf\_S; charge-weighted positive/negative surface area: CASA+/CASA-; Absorption Distribution Metabolism Excretion: ADME; blood–brain barrier: BBB; central nervous system: CNS; permeability-surface area product: logPS; the Salmonella typhimurium reverse mutation assay AMES; potassium channels encoded by hERG genes: hERG; median lethal dose: LD50; aryl hydrogen receptor: AhR; mitochondrial membrane potential: MMP; phosphoprotein tumor suppressor: p53; organic cation transporter 2: OCT2; lysine-specific demethylase 4D: KDM4D; KDM4D-like enzyme: KDM4E.

## References

- Marini, J.J.; Gattinoni, L. Management of COVID-19 Respiratory Distress. *JAMA* **2020**, *323*, 2329. [[CrossRef](#)] [[PubMed](#)]
- Zhu, J.; Ji, P.; Pang, J.; Zhong, Z.; Li, H.; He, C.; Zhang, J.; Zhao, C. Clinical Characteristics of 3062 COVID-19 Patients: A Meta-analysis. *J. Med. Virol.* **2020**, *92*, 1902–1914. [[CrossRef](#)] [[PubMed](#)]
- Sun, H.-L.; Peng, M.-L.; Lee, S.-S.; Chen, C.-J.; Chen, W.-Y.; Yang, M.-L.; Kuan, Y.-H. Endotoxin-Induced Acute Lung Injury in Mice Is Protected by 5,7-Dihydroxy-8-Methoxyflavone via Inhibition of Oxidative Stress and HIF-1 $\alpha$ : Endotoxin induced acute lung injury in mice. *Environ. Toxicol.* **2016**, *31*, 1700–1709. [[CrossRef](#)] [[PubMed](#)]
- Manjili, R.H.; Zarei, M.; Habibi, M.; Manjili, M.H. COVID-19 as an Acute Inflammatory Disease. *J. Immunol.* **2020**, *ji2000413*. [[CrossRef](#)]
- Xu, Z.; Shi, L.; Wang, Y.; Zhang, J.; Huang, L.; Zhang, C.; Liu, S.; Zhao, P.; Liu, H.; Zhu, L.; et al. Pathological Findings of COVID-19 Associated with Acute Respiratory Distress Syndrome. *Lancet Respir. Med.* **2020**, *8*, 420–422. [[CrossRef](#)]
- Pons, S.; Fodil, S.; Azoulay, E.; Zafrani, L. The Vascular Endothelium: The Cornerstone of Organ Dysfunction in Severe SARS-CoV-2 Infection. *Crit. Care* **2020**, *24*, 353. [[CrossRef](#)]
- McGonagle, D.; O'Donnell, J.S.; Sharif, K.; Emery, P.; Bridgewood, C. Immune Mechanisms of Pulmonary Intravascular Coagulopathy in COVID-19 Pneumonia. *Lancet Rheumatol.* **2020**, *2*, e437–e445. [[CrossRef](#)]
- Pan, X.; Li, J.; Tu, X.; Wu, C.; Liu, H.; Luo, Y.; Dong, X.; Li, X.; Pan, L.-L.; Sun, J. Lysine-Specific Demethylase-1 Regulates Fibroblast Activation in Pulmonary Fibrosis via TGF-B1/Smad3 Pathway. *Pharmacol. Res.* **2020**, *152*, 104592. [[CrossRef](#)]
- Tavassoly, I.; Hu, Y.; Zhao, S.; Mariottini, C.; Boran, A.; Chen, Y.; Li, L.; Tolentino, R.E.; Jayaraman, G.; Goldfarb, J.; et al. Genomic Signatures Defining Responsiveness to Allopurinol and Combination Therapy for Lung Cancer Identified by Systems Therapeutics Analyses. *Mol. Oncol.* **2019**, *13*, 1725–1743. [[CrossRef](#)]
- Kayyali, U.S.; Donaldson, C.; Huang, H.; Abdelnour, R.; Hassoun, P.M. Phosphorylation of Xanthine Dehydrogenase/Oxidase in Hypoxia. *J. Biol. Chem.* **2001**, *276*, 14359–14365. [[CrossRef](#)]
- Abrial, C.; Grassin-Delyle, S.; Salvator, H.; Brollo, M.; Naline, E.; Devillier, P. 15-Lipoxygenases Regulate the Production of Chemokines in Human Lung Macrophages: 15-LOXs Affect Production of Chemokines in Lung Macrophages. *Br. J. Pharmacol.* **2015**, *172*, 4319–4330. [[CrossRef](#)] [[PubMed](#)]

12. Selvaraj, G.; Kaliyandurai, S.; Kaushik, A.C.; Khan, A.; Wei, Y.-K.; Cho, W.C.; Gu, K.; Wei, D.-Q. Identification of Target Gene and Prognostic Evaluation for Lung Adenocarcinoma Using Gene Expression Meta-Analysis, Network Analysis and Neural Network Algorithms. *J. Biomed. Inform.* **2018**, *86*, 120–134. [[CrossRef](#)] [[PubMed](#)]
13. Han, Z.; Liao, H.; Shi, F.; Chen, X.; Hu, H.; Tian, M.; Wang, L.; Ying, S. Inhibition of Cyclooxygenase-2 Sensitizes Lung Cancer Cells to Radiation-induced Apoptosis. *Oncol. Lett.* **2017**, *14*, 5959–5965. [[CrossRef](#)] [[PubMed](#)]
14. Park, G.Y.; Christman, J.W. Involvement of Cyclooxygenase-2 and Prostaglandins in the Molecular Pathogenesis of Inflammatory Lung Diseases. *Am. J. Physiol. Lung Cell. Mol. Physiol.* **2006**, *290*, L797–L805. [[CrossRef](#)]
15. Wang, X.; Gray, Z.; Willette-Brown, J.; Zhu, F.; Shi, G.; Jiang, Q.; Song, N.-Y.; Dong, L.; Hu, Y. Macrophage Inducible Nitric Oxide Synthase Circulates Inflammation and Promotes Lung Carcinogenesis. *Cell Death Discov.* **2018**, *4*, 46. [[CrossRef](#)]
16. Betakova, T.; Kostrabova, A.; Lachova, V.; Turianova, L. Cytokines Induced During Influenza Virus Infection. *Curr. Pharm. Des.* **2017**, *23*, 1. [[CrossRef](#)]
17. Chen, G.; Wu, D.; Guo, W.; Cao, Y.; Huang, D.; Wang, H.; Wang, T.; Zhang, X.; Chen, H.; Yu, H.; et al. Clinical and Immunological Features of Severe and Moderate Coronavirus Disease 2019. *J. Clin. Investig.* **2020**, *130*, 2620–2629. [[CrossRef](#)]
18. Rossaint, J.; Nadler, J.L.; Ley, K.; Zarbock, A. Eliminating or Blocking 12/15-Lipoxygenase Reduces Neutrophil Recruitment in Mouse Models of Acute Lung Injury. *Crit. Care* **2012**, *16*, R166. [[CrossRef](#)]
19. Danilov, A.V.; Hu, S.; Orr, B.; Godek, K.; Mustachio, L.M.; Sekula, D.; Liu, X.; Kawakami, M.; Johnson, F.M.; Compton, D.A.; et al. Dinaciclib Induces Anaphase Catastrophe in Lung Cancer Cells via Inhibition of Cyclin-Dependent Kinases 1 and 2. *Mol. Cancer Ther.* **2016**, *15*, 2758–2766. [[CrossRef](#)]
20. Babu, B.R.; Griffith, O.W. Design of Isoform-Selective Inhibitors of Nitric Oxide Synthase. *Curr. Opin. Chem. Biol.* **1998**, *2*, 491–500. [[CrossRef](#)]
21. Morse, J.S.; Lalonde, T.; Xu, S.; Liu, W.R. Learning from the Past: Possible Urgent Prevention and Treatment Options for Severe Acute Respiratory Infections Caused by 2019-nCoV. *ChemBioChem* **2020**, *21*, 730–738. [[CrossRef](#)] [[PubMed](#)]
22. Ortega, J.T.; Serrano, M.L.; Pujol, F.H.; Rangel, H.R. Unrevealing Sequence and Structural Features of Novel Coronavirus Using in Silico Approaches: The Main Protease as Molecular Target. *EXCLI J.* **2020**, *19*, 400–409. [[CrossRef](#)] [[PubMed](#)]
23. Wu, C.; Liu, Y.; Yang, Y.; Zhang, P.; Zhong, W.; Wang, Y.; Wang, Q.; Xu, Y.; Li, M.; Li, X.; et al. Analysis of Therapeutic Targets for SARS-CoV-2 and Discovery of Potential Drugs by Computational Methods. *Acta Pharm. Sin. B* **2020**, *10*, 766–788. [[CrossRef](#)] [[PubMed](#)]
24. Avram, S.; Milac, A.-L.; Borcan, L.-C.; Mihailescu, D.; Borcan, F.; Castanho, M. Designing of Artificial Peptides for an Improved Antiviral Activity. *Curr. Proteom.* **2018**, *15*, 258–266. [[CrossRef](#)]
25. Avram, S.; Puia, A.; Udrea, A.M.; Mihailescu, D.; Mernea, M.; Dinischiotu, A.; Oancea, F.; Stiens, J. Natural Compounds Therapeutic Features in Brain Disorders by Experimental, Bioinformatics and Cheminformatics Methods. *Curr. Med. Chem.* **2020**, *27*, 78–98. [[CrossRef](#)]
26. Zhi, H.-J.; Zhu, H.-Y.; Zhang, Y.-Y.; Lu, Y.; Li, H.; Chen, D.-F. In Vivo Effect of Quantified Flavonoids-Enriched Extract of Scutellaria Aicalensis Root on Acute Lung Injury Induced by Influenza A Virus. *Phytomedicine* **2019**, *57*, 105–116. [[CrossRef](#)]
27. Udrea, A.-M.; Avram, S.; Nistorescu, S.; Pascu, M.-L.; Romanitan, M.O. Laser Irradiated Phenothiazines: New Potential Treatment for COVID-19 Explored by Molecular Docking. *J. Photochem. Photobiol. B Biol.* **2020**, *211*, 111997. [[CrossRef](#)]
28. Zhao, Q.; Chen, X.-Y.; Martin, C. Scutellaria Baicalensis, the Golden Herb from the Garden of Chinese Medicinal Plants. *Sci. Bull.* **2016**, *61*, 1391–1398. [[CrossRef](#)]
29. Zhao, T.; Tang, H.; Xie, L.; Zheng, Y.; Ma, Z.; Sun, Q.; Li, X. *Scutellaria baicalensis* Georgi. (Lamiaceae): A Review of Its Traditional Uses, Botany, Phytochemistry, Pharmacology and Toxicology. *J. Pharm. Pharmacol.* **2019**, *71*, 1353–1369. [[CrossRef](#)]
30. Kim, S.; Chen, J.; Cheng, T.; Gindulyte, A.; He, J.; He, S.; Li, Q.; Shoemaker, B.A.; Thiessen, P.A.; Yu, B.; et al. PubChem 2019 update: Improved access to chemical data. *Nucleic Acids Res.* **2019**, *47*, D1102–D1109. [[CrossRef](#)]

31. Dinda, B.; Dinda, S.; DasSharma, S.; Banik, R.; Chakraborty, A.; Dinda, M. Therapeutic Potentials of Baicalin and Its Aglycone, Baicalein against Inflammatory Disorders. *Eur. J. Med. Chem.* **2017**, *131*, 68–80. [[CrossRef](#)] [[PubMed](#)]
32. Liu, H.; Dong, Y.; Gao, Y.; Du, Z.; Wang, Y.; Cheng, P.; Chen, A.; Huang, H. The Fascinating Effects of Baicalein on Cancer: A Review. *Int. J. Mol. Sci.* **2016**, *17*, 1681. [[CrossRef](#)] [[PubMed](#)]
33. Khan, N.M.; Haseeb, A.; Ansari, M.Y.; Devarapalli, P.; Haynie, S.; Haqqi, T.M. Wogonin, a Plant Derived Small Molecule, Exerts Potent Anti-Inflammatory and Chondroprotective Effects through the Activation of ROS/ERK/Nrf2 Signaling Pathways in Human Osteoarthritis Chondrocytes. *Free. Radic. Biol. Med.* **2017**, *106*, 288–301. [[CrossRef](#)]
34. Shimizu, T.; Shibuya, N.; Narukawa, Y.; Oshima, N.; Hada, N.; Kiuchi, F. Synergistic Effect of Baicalein, Wogonin and Oroxylin A Mixture: Multistep Inhibition of the NF-KB Signalling Pathway Contributes to an Anti-Inflammatory Effect of Scutellaria Root Flavonoids. *J. Nat. Med.* **2018**, *72*, 181–191. [[CrossRef](#)] [[PubMed](#)]
35. Choi, H.J.; Song, H.-H.; Lee, J.-S.; Ko, H.-J.; Song, J.-H. Inhibitory Effects of Norwogonin, Oroxylin A, and Mosloflavone on Enterovirus 71. *Biomol. Ther.* **2016**, *24*, 552–558. [[CrossRef](#)]
36. Song, J.-W.; Long, J.-Y.; Xie, L.; Zhang, L.-L.; Xie, Q.-X.; Chen, H.-J.; Deng, M.; Li, X.-F. Applications, Phytochemistry, Pharmacological Effects, Pharmacokinetics, Toxicity of Scutellaria Baicalensis Georgi. and Its Probably Potential Therapeutic Effects on COVID-19: A Review. *Chin. Med.* **2020**, *15*, 102. [[CrossRef](#)]
37. Song, J.; Zhang, L.; Xu, Y.; Yang, D.; Zhang, L.; Yang, S.; Zhang, W.; Wang, J.; Tian, S.; Yang, S.; et al. The Comprehensive Study on the Therapeutic Effects of Baicalein for the Treatment of COVID-19 In Vivo and In Vitro. *Biochem. Pharmacol.* **2021**, *183*, 114302. [[CrossRef](#)]
38. Russo, M.; Moccia, S.; Spagnuolo, C.; Tedesco, I.; Russo, G.L. Roles of Flavonoids against Coronavirus Infection. *Chemico-Biol. Interact.* **2020**, *328*, 109211. [[CrossRef](#)]
39. Huang, Y.; Zheng, W.; Ni, Y.; Li, M.; Chen, J.; Liu, X.; Tan, X.; Li, J. Therapeutic Mechanism of Toujie Quwen Granules in COVID-19 Based on Network Pharmacology. *BioData Min.* **2020**, *13*, 15. [[CrossRef](#)]
40. Su, H.; Yao, S.; Zhao, W.; Li, M.; Liu, J.; Shang, W.; Xie, H.; Ke, C.; Hu, H.; Gao, M.; et al. Anti-SARS-CoV-2 Activities In Vitro of Shuanghuanglian Preparations and Bioactive Ingredients. *Acta Pharmacol. Sin.* **2020**, *41*, 1167–1177. [[CrossRef](#)]
41. Huang, Y.-F.; Bai, C.; He, F.; Xie, Y.; Zhou, H. Review on the Potential Action Mechanisms of Chinese Medicines in Treating Coronavirus Disease 2019 (COVID-19). *Pharmacol. Res.* **2020**, *158*, 104939. [[CrossRef](#)] [[PubMed](#)]
42. Vilar, S.; Cozza, G.; Moro, S. Medicinal Chemistry and the Molecular Operating Environment (MOE): Application of QSAR and Molecular Docking to Drug Discovery. *Curr. Top. Med. Chem.* **2008**, *8*, 1555–1572. [[CrossRef](#)] [[PubMed](#)]
43. Lipinski, C.A.; Lombardo, F.; Dominy, B.W.; Feeney, P.J. Experimental and Computational Approaches to Estimate Solubility and Permeability in Drug Discovery and Development Settings IPII of Original Article: S0169-409X9600423-1. *Adv. Drug Deliv. Rev.* **2001**, *46*, 3–26. [[CrossRef](#)]
44. Ghose, A.K.; Viswanadhan, V.N.; Wendoloski, J.J. A Knowledge-Based Approach in Designing Combinatorial or Medicinal Chemistry Libraries for Drug Discovery. 1. A Qualitative and Quantitative Characterization of Known Drug Databases. *J. Comb. Chem.* **1999**, *1*, 55–68. [[CrossRef](#)]
45. Veber, D.F.; Johnson, S.R.; Cheng, H.-Y.; Smith, B.R.; Ward, K.W.; Kopple, K.D. Molecular Properties That Influence the Oral Bioavailability of Drug Candidates. *J. Med. Chem.* **2002**, *45*, 2615–2623. [[CrossRef](#)]
46. Egan, W.J.; Merz, K.M.; Baldwin, J.J. Prediction of Drug Absorption Using Multivariate Statistics. *J. Med. Chem.* **2000**, *43*, 3867–3877. [[CrossRef](#)]
47. Daina, A.; Michielin, O.; Zoete, V. SwissADME: A Free Web Tool to Evaluate Pharmacokinetics, Drug-Likeness and Medicinal Chemistry Friendliness of Small Molecules. *Sci. Rep.* **2017**, *7*, 42717. [[CrossRef](#)]
48. Udrea, A.-M. Computational Approaches of New Perspectives in the Treatment of Depression during Pregnancy. *Farmacia* **2018**, *66*, 680–687. [[CrossRef](#)]
49. Wood, D.J.; De Vlieg, J.; Wagener, M.; Ritschel, T. Pharmacophore Fingerprint-Based Approach to Binding Site Subpocket Similarity and its Application to Bioisostere Replacement. *J. Chem. Inf. Model.* **2012**, *52*, 2031–2043. [[CrossRef](#)]
50. Rácz, A.; Bajusz, D.; Héberger, K. Life beyond the Tanimoto Coefficient: Similarity Measures for Interaction Fingerprints. *J. Cheminform.* **2018**, *10*, 48. [[CrossRef](#)]

51. Daina, A.; Michielin, O.; Zoete, V. SwissTargetPrediction: Updated Data and New Features for Efficient Prediction of Protein Targets of Small Molecules. *Nucleic Acids Res.* **2019**, *47*, W357–W364. [[CrossRef](#)] [[PubMed](#)]
52. Bank, R.P.D. RCSB PDB—6M2N: SARS-CoV-2 3CL Protease (3CL pro) in Complex with a Novel Inhibitor. Available online: <https://www.rcsb.org/structure/6M2N> (accessed on 13 October 2020).
53. Grosdidier, A.; Zoete, V.; Michielin, O. SwissDock, a Protein–Small Molecule Docking Web Service Based on EADock DSS. *Nucleic Acids Res.* **2011**, *39* (Suppl. 2), W270–W277. [[CrossRef](#)] [[PubMed](#)]
54. Grosdidier, A.; Zoete, V.; Michielin, O. Fast Docking Using the CHARMM Force Field with EADock DSS. *J. Comput. Chem.* **2011**, *32*, 2149–2159. [[CrossRef](#)] [[PubMed](#)]
55. Pettersen, E.F.; Goddard, T.D.; Huang, C.C.; Couch, G.S.; Greenblatt, D.M.; Meng, E.C.; Ferrin, T.E. UCSF Chimera—A Visualization System for Exploratory Research and Analysis. *J. Comput. Chem.* **2004**, *25*, 1605–1612. [[CrossRef](#)] [[PubMed](#)]
56. Hastings, J.; Owen, G.; Dekker, A.; Ennis, M.; Kale, N.; Muthukrishnan, V.; Turner, S.; Swainston, N.; Mendes, P.; Steinbeck, C. ChEBI in 2016: Improved Services and an Expanding Collection of Metabolites. *Nucleic Acids Res.* **2016**, *44*, D1214–D1219. [[CrossRef](#)] [[PubMed](#)]
57. Laskowski, R.A.; Swindells, M.B. LigPlot+: Multiple Ligand–Protein Interaction Diagrams for Drug Discovery. *J. Chem. Inf. Model.* **2011**, *51*, 2778–2786. [[CrossRef](#)] [[PubMed](#)]
58. Pires, D.E.V.; Blundell, T.L.; Ascher, D.B. PkCSM: Predicting Small-Molecule Pharmacokinetic and Toxicity Properties Using Graph-Based Signatures. *J. Med. Chem.* **2015**, *58*, 4066–4072. [[CrossRef](#)]
59. Drwal, M.N.; Banerjee, P.; Dunkel, M.; Wettig, M.R.; Preissner, R. ProTox: A Web Server for the in Silico Prediction of Rodent Oral Toxicity. *Nucleic Acids Res.* **2014**, *42*, W53–W58. [[CrossRef](#)]
60. Lovering, F.; Bikker, J.; Humblet, C. Escape from Flatland: Increasing Saturation as an Approach to Improving Clinical Success. *J. Med. Chem.* **2009**, *52*, 6752–6756. [[CrossRef](#)]
61. Chen, H.; Guan, B.; Chen, X.; Chen, X.; Li, C.; Qiu, J.; Yang, D.; Liu, K.J.; Qi, S.; Shen, J. Baicalin Attenuates Blood–Brain Barrier Disruption and Hemorrhagic Transformation and Improves Neurological Outcome in Ischemic Stroke Rats with Delayed t-PA Treatment: Involvement of ONOO-MMP-9 Pathway. *Transl. Stroke Res.* **2018**, *9*, 515–529. [[CrossRef](#)]
62. Shin, J.-W.; Kang, H.-C.; Shim, J.; Sohn, N.-W. Scutellaria Baicalensis Attenuates Blood–Brain Barrier Disruption after Intracerebral Hemorrhage in Rats. *Am. J. Chin. Med.* **2012**, *40*, 85–96. [[CrossRef](#)] [[PubMed](#)]
63. Li, T.; Li, N.; Guo, Q.; Ji, H.; Zhao, D.; Xie, S.; Li, X.; Qiu, Z.; Han, D.; Chen, X.; et al. Inhibitory Effects of Wogonin on Catalytic Activity of Cytochrome P450 Enzyme in Human Liver Microsomes. *Eur. J. Drug Metab. Pharmacokinet.* **2011**, *36*, 249–256. [[CrossRef](#)] [[PubMed](#)]
64. Liao, Y.; Yang, Y.; Wang, X.; Wei, M.; Guo, Q.; Zhao, L. Oroxyloside Ameliorates Acetaminophen-Induced Hepatotoxicity by Inhibiting JNK Related Apoptosis and Necroptosis. *J. Ethnopharmacol.* **2020**, *258*, 112917. [[CrossRef](#)] [[PubMed](#)]
65. Zhang, L.; Lin, D.; Sun, X.; Curth, U.; Drosten, C.; Sauerhering, L.; Becker, S.; Rox, K.; Hilgenfeld, R. Crystal Structure of SARS-CoV-2 Main Protease Provides a Basis for Design of Improved  $\alpha$ -Ketoamide Inhibitors. *Science* **2020**, *368*, 409–412. [[CrossRef](#)]
66. Uhlén, M.; Fagerberg, L.; Hallström, B.M.; Lindskog, C.; Oksvold, P.; Mardinoglu, A.; Sivertsson, Å.; Kampf, C.; Sjöstedt, E.; Asplund, A.; et al. Tissue-based map of the human proteome. *Science* **2015**, *347*, 1260419. [[CrossRef](#)]
67. Labbé, R.M.; Holowatyj, A.; Yang, Z.-Q. Histone Lysine Demethylase (KDM) Subfamily 4: Structures, Functions and Therapeutic Potential. *Am. J. Transl. Res.* **2013**, *6*, 1–15.
68. Saul, D.; Weber, M.; Zimmermann, M.H.; Kosinsky, R.L.; Hoffmann, D.B.; Menger, B.; Taudien, S.; Lehmann, W.; Komrakova, M.; Sehmisch, S. Effect of the Lipoygenase Inhibitor Baicalein on Bone Tissue and Bone Healing in Ovariectomized Rats. *Nutr. Metab. Lond* **2019**, *16*, 4. [[CrossRef](#)]
69. Hsu, S.-L.; Hsieh, Y.-C.; Hsieh, W.-C.; Chou, C.-J. Baicalein Induces a Dual Growth Arrest by Modulating Multiple Cell Cycle Regulatory Molecules. *Eur. J. Pharmacol.* **2001**, *425*, 165–171. [[CrossRef](#)]
70. Avram, S.; Bologa, C.G.; Holmes, J.; Bocci, G.; Wilson, T.B.; Nguyen, D.-T.; Curpan, R.; Halip, L.; Bora, A.; Yang, J.J.; et al. DrugCentral 2021 supports drug discovery and repositioning. *Nucleic Acids Res.* **2020**, gkaa997. [[CrossRef](#)]

71. Ni, T.; He, Z.; Dai, Y.; Yao, J.; Guo, Q.; Wei, L. Oroxylin A Suppresses the Development and Growth of Colorectal Cancer through Reprogram of HIF1 $\alpha$ -Modulated Fatty Acid Metabolism. *Cell Death Dis.* **2017**, *8*, e2865. [[CrossRef](#)]
72. Chen, Y.-C.; Shen, S.-C.; Chen, L.-G.; Lee, T.J.-F.; Yang, L.-L. Wogonin, Baicalin, and Baicalein Inhibition of Inducible Nitric Oxide Synthase and Cyclooxygenase-2 Gene Expressions Induced by Nitric Oxide Synthase Inhibitors and Lipopolysaccharide11. *Biochem. Pharmacol.* **2001**, *61*, 1417–1427. [[CrossRef](#)]
73. Kim, H.P.; Son, K.H.; Chang, H.W.; Kang, S.S. Anti-Inflammatory Plant Flavonoids and Cellular Action Mechanisms. *J. Pharmacol. Sci.* **2004**, *96*, 229–245. [[CrossRef](#)] [[PubMed](#)]
74. Fang, Y.; Yang, C.; Yu, Z.; Li, X.; Mu, Q.; Liao, G.; Yu, B. Natural Products as LSD1 Inhibitors for Cancer Therapy. *Acta Pharm. Sin. B* **2020**, in press. [[CrossRef](#)] [[PubMed](#)]
75. Zheng, Y.-C.; Shen, D.-D.; Ren, M.; Liu, X.-Q.; Wang, Z.-R.; Liu, Y.; Zhang, Q.-N.; Zhao, L.-J.; Zhao, L.-J.; Ma, J.-L.; et al. Baicalin, a Natural LSD1 Inhibitor. *Bioorganic Chem.* **2016**, *69*, 129–131. [[CrossRef](#)] [[PubMed](#)]

**Publisher’s Note:** MDPI stays neutral with regard to jurisdictional claims in published maps and institutional affiliations.



© 2020 by the authors. Licensee MDPI, Basel, Switzerland. This article is an open access article distributed under the terms and conditions of the Creative Commons Attribution (CC BY) license (<http://creativecommons.org/licenses/by/4.0/>).